



Cite this: DOI: 10.1039/d1se00819f

# A multiple laser-induced hybrid electrode for flexible triboelectric nanogenerators†

Huamin Chen,<sup>ab</sup> Wei Yang,<sup>a</sup> Peiyu Huang,<sup>a</sup> Chenyu Li,<sup>a</sup> Yaqian Yang,<sup>a</sup> Biao Zheng,<sup>a</sup> Cheng Zhang,<sup>a</sup> Ruping Liu,<sup>e</sup> Yuliang Li,<sup>a</sup> Yun Xu,<sup>cd</sup> Jun Wang<sup>\*a</sup> and Zhou Li<sup>bf</sup>

Triboelectric nanogenerators (TENGs) stand out from wearable energy-harvesting technologies due to their high output power and flexibility. Moreover, triboelectric materials particularly the electrodes are considered to be the most significant part, which directly affect the output, flexibility and the fabrication process. In this study, we propose the fabrication of a laser-induced graphene (LIG)-Au hybrid electrode-based flexible TENG by a simple laser-induced method. Utilizing multiple laser irradiation, the PI and metal precursor can be induced to form a porous Au-LIG hybrid electrode. The Au nanoparticles on porous LIG are uniform and dense. Furthermore, this simple method can control the concentration and pattern of the Au-LIG flexible electrode. Based on the Au-LIG flexible electrode, we fabricated a flexible TENG and investigated the effects of the Au concentration on the output performance. The maximum instantaneous power of the Au-LIG-based TENG increased about 4 times compared to that of the LIG-based TENG. Finally, we developed a TENG-based sensor for writing recognition. According to the voltage signal and signal order, we can refer the writing track. This cost-effective method can fabricate the flexible electrode with enhanced performance, which paves the development of flexible and wearable electronics.

Received 30th May 2021  
Accepted 15th June 2021

DOI: 10.1039/d1se00819f

rsc.li/sustainable-energy

## 1 Introduction

Flexible and stretchable electronics have received considerable attention with the rapid development of internet of things (IoT).<sup>1–5</sup> It has numerous inherent advantages for applications such as health monitoring and big data capturing.<sup>6–9</sup> However, the limitation of power unit including batteries in rigidity, weight and volume, are not suitable for powering wearable sensors. It is a promising strategy to incorporate the wearable energy-harvesting technology with flexible electronics for realizing self-powered systems. Energy-harvesting devices have made remarkable progress in recent decades including piezoelectric nanogenerators,<sup>10,11</sup> thermoelectric nanogenerators,<sup>12,13</sup> and particularly triboelectric nanogenerators (TENGs).<sup>14,15</sup>

TENGs based on the contact electrification and electrostatic induction can efficiently harvest the mechanical energy from human routine activities compared to other nanogenerators.<sup>16,17</sup> On account of its high efficiency,<sup>18</sup> simple construction,<sup>19</sup> and flexibility,<sup>20</sup> it has become the most promising candidate for future power source.

Triboelectric materials particularly the electrodes are considered to be the most significant part, which directly affect the output, flexibility and the fabrication process. To date, various materials have been applied for the electrode/tri-triboelectric layer including metal/metallic composites and carbon/carbon composites.<sup>21–23</sup> The metallic electrodes usually prepared by the vacuum deposition method are expensive. Furthermore, the adhesive process can cause poor bonding between the electrode/dielectric layer, which greatly affects the durability and output of TENGs for long-term bending or stretching cycles. In contrast, carbon-based electrodes are usually prepared by self-assembly,<sup>24,25</sup> coating,<sup>26,27</sup> or vacuum filtration.<sup>28,29</sup> Through these synthetic methods, they can achieve a porous and three-dimensional (3D) structure,<sup>30,31</sup> which is beneficial for enhancing the output of TENGs. In 2014, Lin *et al.* demonstrated a novel method to synthesize 3D graphene *via* laser irradiation on the carbon source such as polyimide (PI).<sup>32</sup> This straightforward synthesis of laser-induced graphene (LIG) has advantages such as simple fabrication process, easy patterning and scalable production, which make it suitable for flexible electrodes.<sup>33–35</sup>

<sup>a</sup>Fujian Key Laboratory of Functional Marine Sensing Materials, Center for Advanced Marine Materials and Smart Sensors, Minjiang University, Fuzhou, 350108, China. E-mail: wangjun2@mju.edu.cn

<sup>b</sup>CAS Center for Excellence in Nanoscience, Beijing Key Laboratory of Micro-nano Energy and Sensor, Beijing Institute of Nanoenergy and Nanosystems, Chinese Academy of Sciences, Beijing 100083, China. E-mail: zli@binn.cas.cn

<sup>c</sup>Institute of Semiconductors, Chinese Academy of Sciences, Beijing 100083, China

<sup>d</sup>Beijing Key Laboratory of Inorganic Stretchable and Flexible Information Technology, Beijing 100083, China

<sup>e</sup>Beijing Institute of Graphic Communication, Beijing, 102600, China

<sup>f</sup>School of Nanoscience and Technology, University of Chinese Academy of Sciences, Beijing 100049, China

† Electronic supplementary information (ESI) available. See DOI: 10.1039/d1se00819f

To improve the performance of LIG-based electrodes, active nanoparticles are incorporated into the LIG to construct hybrid materials.<sup>36,37</sup> However, to the best of our knowledge, methods such as laser induction<sup>38</sup> and electrochemical deposition,<sup>39,40</sup> are time-consuming and need complex formulation and equipment. Moreover, the LIG electrode is usually used as the back electrode,<sup>41–43</sup> which does not participate directly in the friction process.

In this study, we proposed an Au-LIG hybrid electrode-based flexible TENG by a multiple laser-induced method. First, the PI substrate was irradiated by a laser to convert the carbon source to porous graphene. The metal precursor of Au nanoparticles was then spin-coated on the LIG, followed by a second laser irradiation to form an Au-LIG hybrid electrode. The Au nanoparticles on porous LIG were uniform and dense. Furthermore, this method can control the concentration and pattern of the Au-LIG flexible electrode. Based on the Au-LIG flexible electrode, we fabricated a flexible TENG and investigated the effects of the Au concentration on the output performance. Finally, we developed a flexible TENG-based sensor for writing recognition. This cost-effective method can fabricate flexible electrodes with enhanced performance, which paves the way for the development of flexible and wearable electronics.

## 2 Experimental

### 2.1 Fabrication of the Au-LIG hybrid electrode

Gold chloride trihydrate ( $\text{HAuCl}_4$ ) was purchased from Sino-pharm (China). Polydimethylsiloxane (PDMS, Sylgard 184) was

purchased from Dow Corning (USA). A polyimide (PI) tape with a thickness of 100  $\mu\text{m}$  was purchased from Dupont (USA).

First, the PI tape was irradiated by a computer-controlled  $\text{CO}_2$  infrared laser. By adjusting the parameters including geometries, power, scan speed and depth, we can control the pattern of LIG. The  $\text{HAuCl}_4$  aqueous solution with different concentrations (0.1  $\text{mg mL}^{-1}$ , 0.2  $\text{mg mL}^{-1}$ , 0.3  $\text{mg mL}^{-1}$ , 0.4  $\text{mg mL}^{-1}$ , and 0.5  $\text{mg mL}^{-1}$ ) was then spin-coated on the LIG surface at 200 rpm for 5 s (spin coater, KW-4A) and then dried at 70  $^\circ\text{C}$  for 5 min. Finally, the LIG coated with  $\text{HAuCl}_4$  was re-irradiated by a laser scribing system (Nano Pro-III, China).  $\text{HAuCl}_4$  was reduced to Au nanoparticles, which was strongly attached to LIG.

### 2.2 Construction of the flexible TENG and writing sensor

The Au-LIG hybrid electrode was patterned by the laser scribing system and the side length of the square was 1.8 cm. The uncured PDMS (base/curing agent was mixed at a weight ratio of 10 : 1) was poured on the Au-LIG electrode. After spinning at 1200 rpm for 10 s, it was then cured at 80  $^\circ\text{C}$  for 1 h. The PDMS film acts as a dielectric layer with a thickness of 0.2 mm. The upper PI/Au-LIG/PDMS film and the bottom PI/Au-LIG film were connected by the PDMS spacer with a distance of 5 mm.

### 2.3 Characterization

The surface morphologies of the as-prepared samples were obtained by a 3D laser scanning microscope (VK-X200 series) and field emission scanning electron microscope (SEM, EMIST-7). The Raman spectra were recorded by a spectrograph (Horiba

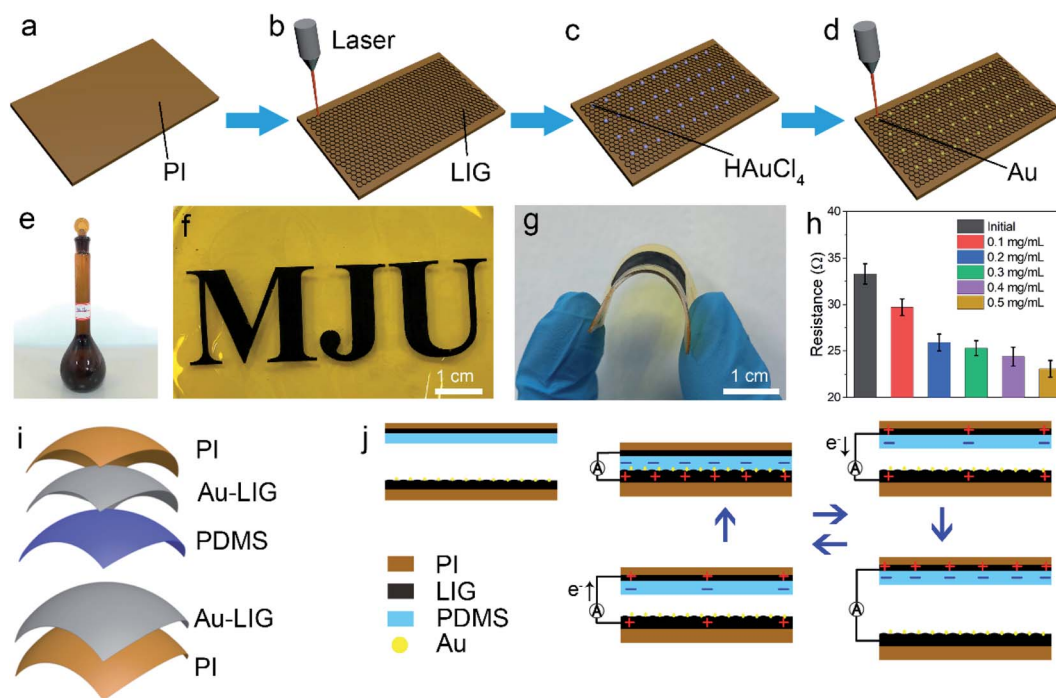


**Fig. 1** Schematic of the fabrication process and device structure of the TENG; (a) the PI substrate; (b) the LIG on the PI substrate; (c)  $\text{HAuCl}_4$  spin-coated on the LIG; (d) irradiation; (e) the image of the  $\text{HAuCl}_4$ . (f) The MJU image of the Au-LIG electrode. (g) The flexible LIG electrode; (h) the resistance of the Au-LIG electrode with various concentrations; (i) the schematic of the device structure; (j) the working mechanism of the TENG.

HR Evolution 800). The elemental analysis was carried out on an energy dispersive spectrometer (EDS, X-MaxN50). The experimental parameters of the compressive force and the frequency were controlled by a linear motor position system. Also, the output performance was characterized by an electrometer (Keithley 6514).

### 3 Results and discussion

The schematic of the synthesis process of the Au-LIG electrode is illustrated in Fig. 1a–d. After irradiating the PI carbon source, a layer of the porous carbon film was fabricated. The  $\text{HAuCl}_4$  aqueous solution was then spin-coated on the LIG surface, followed by second irradiation on the LIG surface. After that,  $\text{Au}^{3+}$  could be reduced to stable Au nanoparticles, which were tightly and uniformly distributed on the LIG surface. This method can simply and effectively introduce active nanoparticles such as noble metals into LIG to improve its physical and chemical properties. The photographs of the  $\text{HAuCl}_4$  solution and the Au-LIG electrode are shown in Fig. 1e and f. The LIG can be designed in various patterns such as “MJU”. The line width of Au-LIG is 10  $\mu\text{m}$ . Due to the flexibility of PI, it can bend and twist, as shown in Fig. 1g. Also, the resistances of the Au-LIG electrode at various concentrations are compared in Fig. 1h. The resistance of the initial LIG without Au nanoparticles was about 33  $\Omega$ . Also, the resistance was decreased to 20  $\Omega$  as the concentration increased to 0.5  $\text{mg mL}^{-1}$ . The Au-LIG hybrid material is a promising electrode for flexible TENGs. The schematic structure of the flexible TENG is displayed in Fig. 1i.

Au-LIG on the bottom PI substrate acts as the triboelectric material as well as the bottom electrode. The Au-LIG electrode between the PI and dielectric layer PDMS is the back electrode. Fig. 1j illustrates the working mechanism of the flexible TENG. During the contact-separation process, the electron can flow between the two Au-LIG electrodes.

To analyse the morphologies and chemical properties of the Au-LIG electrode, the SEM, Raman spectroscopy and EDS were carried out and the results are shown in Fig. 2. As shown in Fig. 2a, the Au-LIG electrode obviously has a porous structure and the porous size is about micro scale. As shown in the higher resolution SEM image in Fig. 2b, the Au nanoparticles are uniformly distributed on the porous LIG surface in a large scale. The further higher resolution SEM in Fig. 2c can clearly exhibit that the Au nanoparticles are tightly and densely decorated on the porous LIG. Also, we can obviously find the Au nanoparticles on the LIG surface and interior. The effects of synthesis parameters such as laser power and  $\text{HAuCl}_4$  concentration on the properties of Au-LIG were also investigated. First, the effects of the laser power on the morphologies of LIG and Au-LIG were studied. As shown in Fig. S1,<sup>†</sup> the SEM images showed that the porous LIG became curlier at a high laser power. The most suitable power was 4.4 W at the scan depth of 10  $\mu\text{m}$ . At the laser power of 4.4 W with the depth of 10  $\mu\text{m}$ , the effects of the  $\text{HAuCl}_4$  concentration on the size of the Au nanoparticles were explored. The SEM images in Fig. S2<sup>†</sup> exhibited that the size of Au nanoparticles became larger and the distribution of Au nanoparticles on the LIG became denser. The Raman spectra of  $\text{HAuCl}_4$ -LIG and Au-LIG are shown in Fig. 2d. The D, G, and 2D

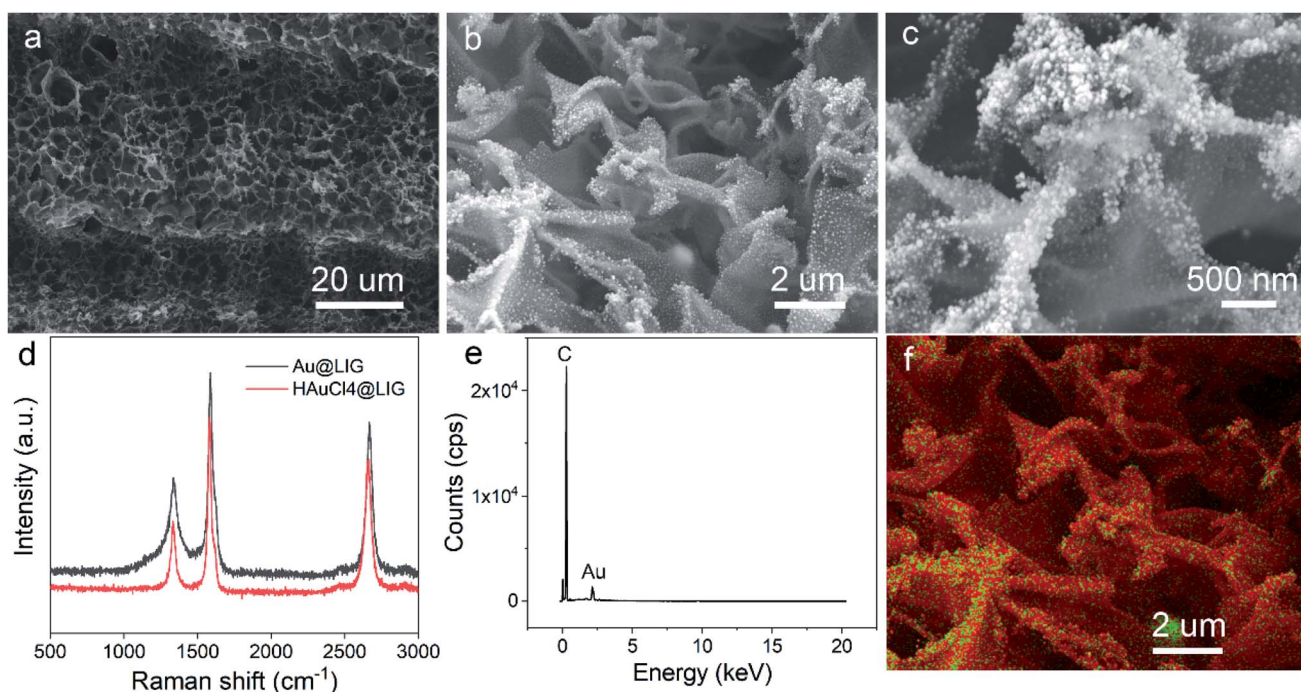


Fig. 2 The morphologies and elemental analysis of the Au-LIG hybrid electrode. (a) The SEM image of the porous electrode. (b) The higher resolution SEM of the Au nanoparticles distributed on the LIG. (c) The higher resolution SEM of the Au nanoparticles. (d) The Raman spectra of the Au-LIG electrode and  $\text{HAuCl}_4$ -LIG electrode. (e) The energy dispersive X-ray spectroscopy (EDS) of the Au-LIG electrode. (f) The EDS mapping of the Au-LIG electrode.

peaks are at  $1332\text{ cm}^{-1}$ ,  $1587\text{ cm}^{-1}$ , and  $2665\text{ cm}^{-1}$ , respectively, which correspond to the graphene. The EDS of Au-LIG is displayed in Fig. 2e. As seen from the curve, C, Au and Si (the substrate) elements are there in the Au-LIG electrode, and the atomic percentage indicate that most Au was in the metallic state. The EDS mapping of Au-LIG in Fig. 2f also clearly shows that the Au nanoparticles are evenly distributed in LIG. Also, the detailed EDS mapping is shown in Fig. S3.†

To evaluate the performance of the TENG based on the Au-LIG hybrid electrode, the effects of the Au concentration, compressive force and working frequencies on the transferred charge, output voltage and current were investigated in Fig. 3. A series of TENGs based on the Au-LIG electrode at various concentrations was constructed. The output performance of TENG was measured under a compressive force of 30 N at a frequency of 1 Hz. As shown in Fig. 3a, the transferred charge density of the initial LIG-based TENG was 1.9 nC. The transferred charge densities of the TENGs at various concentrations

(0.1  $\text{mg mL}^{-1}$ , 0.2  $\text{mg mL}^{-1}$ , 0.3  $\text{mg mL}^{-1}$ , 0.4  $\text{mg mL}^{-1}$ , and 0.5  $\text{mg mL}^{-1}$ ) were 2.9 nC, 3.8 nC, 4.6 nC, 6.8 nC, and 7.6 nC, respectively.

The transferred charge of Au-LIG-based TENG (0.5  $\text{mg mL}^{-1}$ ) increased about 4 times compared to that of the LIG-based TENG. Also, the corresponding output voltages of these TENGs were 8.1 V, 10.8 V, 12.5 V, 14.1 V, 21.5 V, and 25.6 V, respectively. The output voltage increased about 3 times, as presented in Fig. 3b. The corresponding output currents were 0.4  $\mu\text{A}$ , 1.0  $\mu\text{A}$ , 1.7  $\mu\text{A}$ , 2.6  $\mu\text{A}$ , 3.3  $\mu\text{A}$ , and 4.4  $\mu\text{A}$ , respectively. The effects of the compressive force on the output performance are presented in Fig. 3d-f. The output performance of the TENG was measured at a frequency of 1 Hz under various compressive forces. As displayed in Fig. 3d, the transferred charge increased as the compressive force increased from 5 N to 50 N. The transferred charge of TENG under 50 N increased about 2 times compared to that of TENG under 5 N. The output voltage in Fig. 3e and the output current in Fig. 3f exhibit the similar trend.

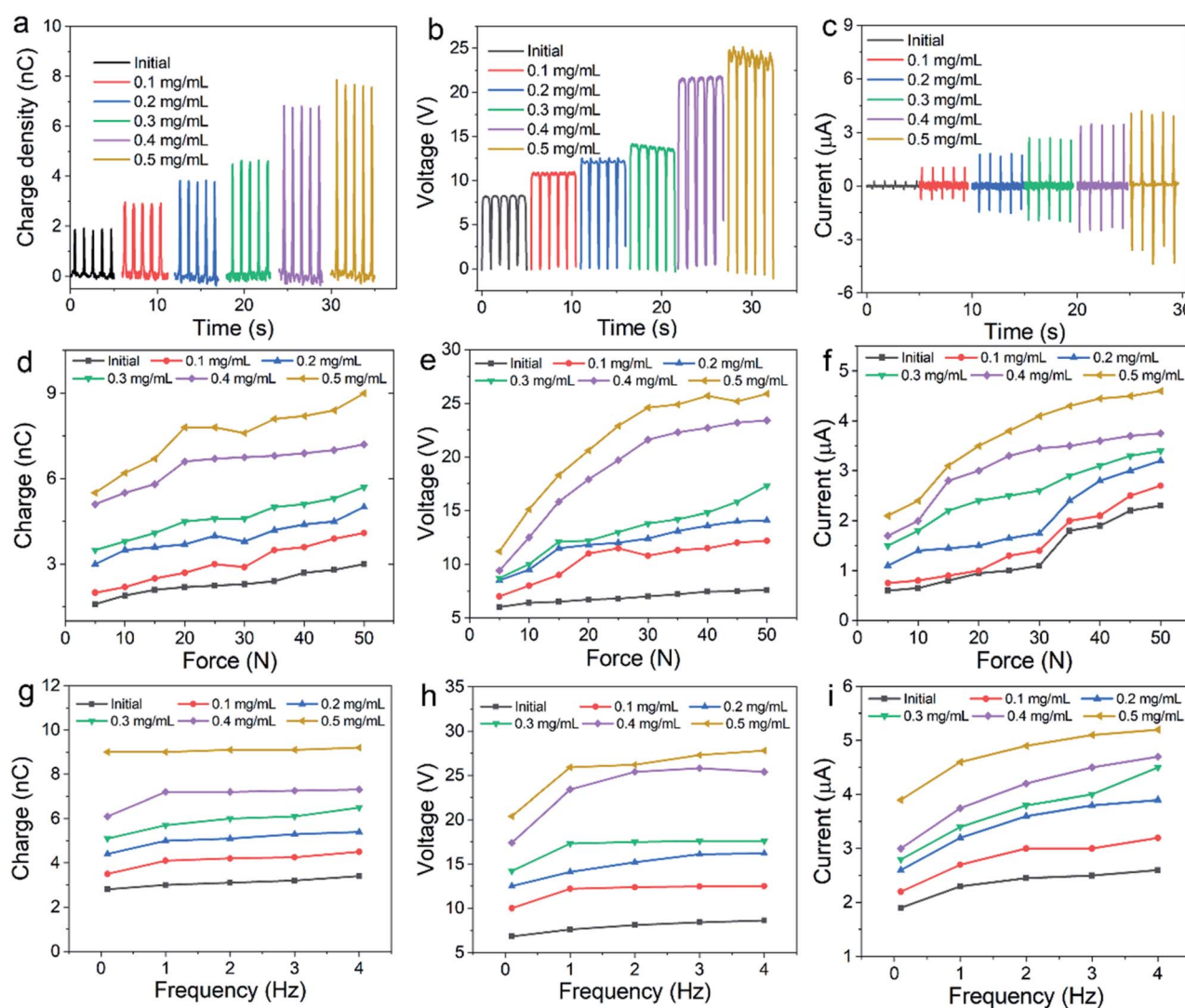


Fig. 3 The output performance of the TENGs. (a) The transferred charge, (b) output voltage, and (c) output current of the TENG with various Au concentrations. (d) The transferred charge, (e) output voltage, and (f) output current of the TENG under different compressive forces. (g) The transferred charge, (h) output voltage, and (i) output current of the TENG at different frequencies.

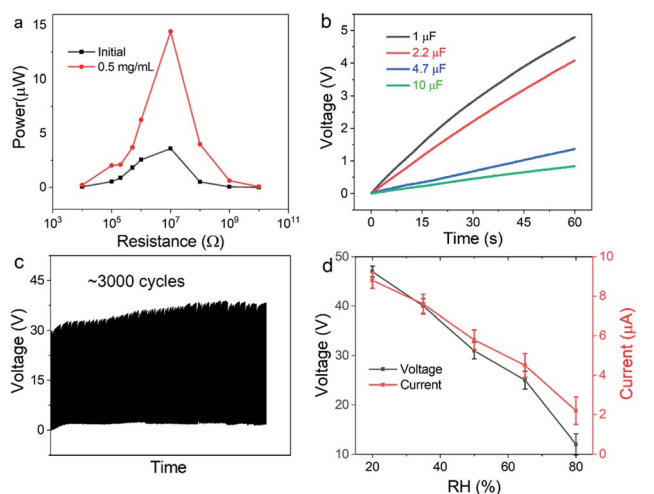


Fig. 4 The charging ability of the TENG. (a) The comparison of the power of LIG-based TENG and Au-LIG-based TENG. (b) The charging ability of the Au-LIG-based TENG. (c) The stability test of the TENG. (d) The relationship between the output performance and the RH.

The relationship between the output performance and the working frequency is presented in Fig. 3g–i. The performance of TENG was measured under a compressive force of 50 N. It is obvious that the transferred charge did not increase when the frequency increased from 0.1 Hz to 4 Hz. This is because the speed of the contact-separation motion hardly affects the amount of the transferred charge. In contrary, the output voltage and current increased slowly as the frequency increased from 0.1 Hz to 4 Hz. This is due to the faster electron transfer speed.

The powering ability is an important parameter to evaluate its potential for future energy source. The relationship of the instantaneous power with the load resistance is shown in Fig. 4a. The maximum instantaneous power of the LIG-based TENG was 3.6  $\mu\text{W}$  at a resistance of 10 M $\Omega$ . Also, the maximum instantaneous power of the Au-LIG-based TENG was 14.4  $\mu\text{W}$ , which was increased about 4 times. The charging curves of the various capacitors are presented in Fig. 4b. The capacitor of 1  $\mu\text{F}$  can be charged to 5 V in 1 min, which demonstrated the potential for powering wearable electronics. The stability test of the TENG (2 cm  $\times$  2 cm) was conducted and the results are shown in Fig. 4c. The

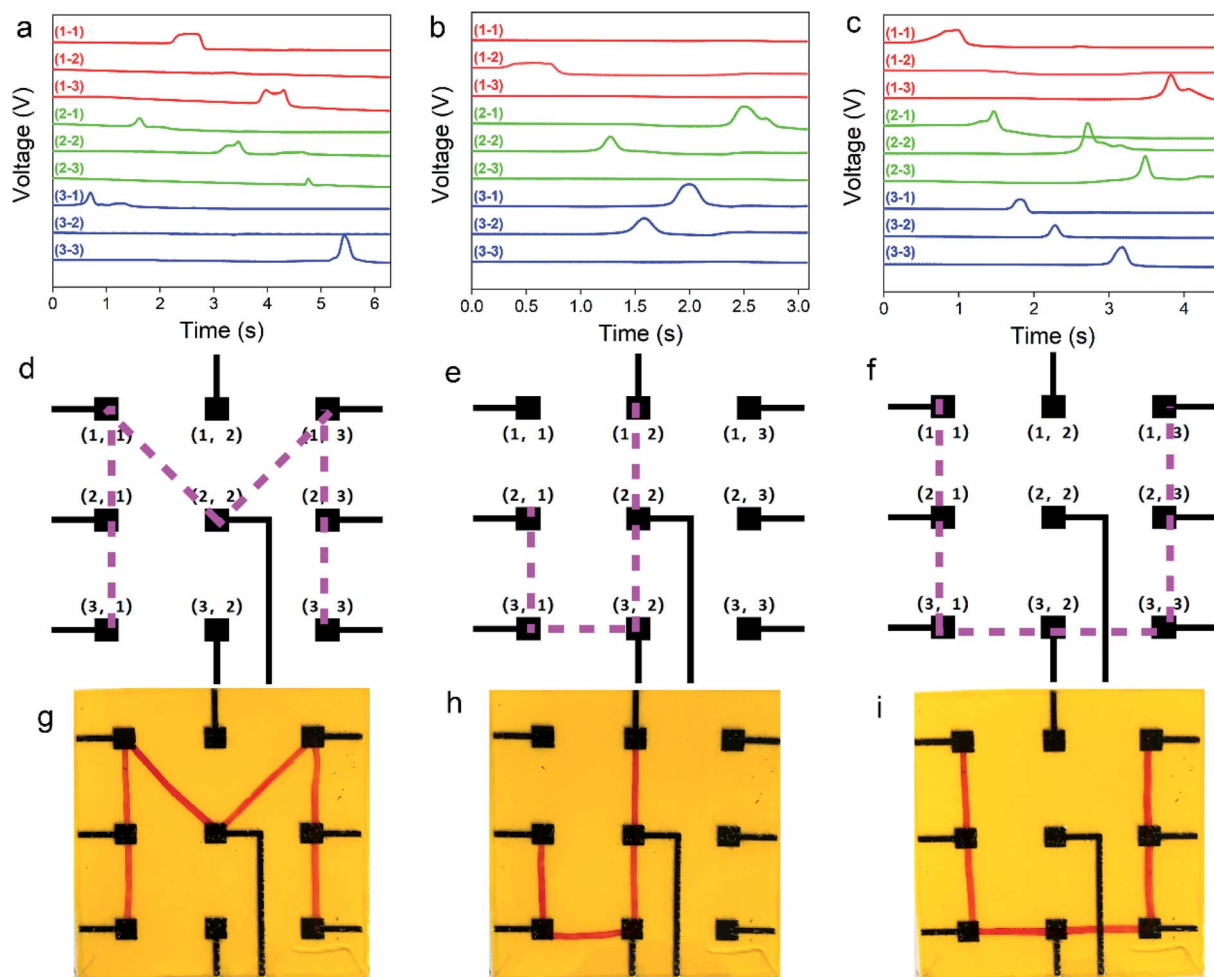


Fig. 5 The application of the TENG for writing recognition. (a)–(c) The voltage signals of the TENG array. (d)–(f) The writing pattern of the TENG array. (g)–(i) The image of the "MJU" samples.

output voltage was measured under the compressive force of 50 N at a frequency of 1 Hz and a relatively humidity (RH) of 50%. As the charge gets saturated, the output voltage remains stable at about 38 V. Considering the high RH of 50% in this experiment, we also measured the output performance of TENG under various RH. As shown in Fig. 4d, the output voltage rapidly increased from 12 V to 47 V as the RH decreased from 80% to 30%. Moreover, the output current increased from 2.2  $\mu$ A to 8.8  $\mu$ A, which indicates that higher performance can be obtained in a dry environment.

The Au-LIG hybrid electrode has the advantage of simple fabrication and can be easily patterned. Therefore, we fabricated a  $3 \times 3$  electrode array for writing sensors. After fabricating the Au-LIG electrode, a PDMS solution with a base/curing agent weight ratio of 20 : 1 was spin-coated on the Au-LIG electrode and cured at 80 °C for 1 h. The Au-LIG/PDMS writing board was flexible and transparent. The writing sensor based on the TENG works under a single-electrode mode. PDMS acts as the negative triboelectric material and the pen acts as the positive triboelectric material. When the pencil sweeps on PDMS, electrostatic charges are generated and distribute on the PDMS and the active object. As the pen moves on the PDMS surface, a potential difference forms between the Au-LIG electrode and the ground. The potential difference between the Au-LIG electrode and the ground can drive the electron flow between the two electrodes. An obvious voltage signal can generate when the pen is on the electrode. Also, when the pencil leaves the electrode, there is nearly no signal, as shown in Fig. 5a–c. According to the voltage signal and signal order, we can refer the writing track. Fig. 5d–f present the schematic electrode pattern and the writing track of “MJU”. Moreover, the images of the “MJU” are shown in Fig. 5g–i. This application demonstrated that this TENG is not only suitable for harvesting wasted energy, but also promising for sensing and recognition.

## 4 Conclusion

In summary, we proposed an Au-LIG hybrid electrode-based flexible TENG *via* a simple laser-induced method. Utilizing multiple laser irradiation, the PI and metal precursor can be induced to form a porous Au-LIG hybrid electrode. The Au nanoparticles on porous LIG were uniform and dense. Furthermore, this simple method can control the concentration and pattern of the Au-LIG flexible electrode. Based on the Au-LIG flexible electrode, we fabricated a flexible TENG and investigated the effects of the Au concentration on the output performance. The maximum instantaneous power of the Au-LIG-based TENG was 14.4  $\mu$ W, which increased about 4 times. Finally, we developed a TENG-based sensor for writing recognition. According to the voltage signal and signal order, we can refer the writing track. This cost-effective method can fabricate flexible electrodes with enhanced performance, which would pave the way for the development of flexible and wearable electronics.

## Author contributions

Huamin Chen: conceptualization, formal analysis, writing – original draft, funding acquisition. Wei Yang: data curation,

visualization, investigation. Peiyu Huang: investigation. Chenyu Li: data curation. Yaqian Yang: investigation. Biao Zheng: software. Cheng Zhang: formal analysis, investigation. Ruping Liu: funding acquisition. Yuliang Li: validation, visualization. Yun Xu: writing – review & editing. Jun Wang: validation, resources, supervision. Zhou Li: funding acquisition, project administration.

## Conflicts of interest

There are no conflicts to declare.

## Acknowledgements

This work was supported by the National Natural Science Foundation of China (No. 11674185, 61875015, 61971049), the Natural Science Foundation of Fujian (No. 2020J01857, 2019J01764), the Fuzhou City Science and Technology Cooperation Project (2020-GX-5, 2020-S-29), Beijing Natural Science Foundation (JQ20038), the Key Scientific Research Project of Beijing Municipal Commission of Education (KZ202010015024), the Research and Development Program of Beijing Institute of Graphic Communication (Ec202006), the Beijing Municipal Science and Technology Commission (Z181100004418004).

## Notes and references

- 1 Y. Chen, Y. Zhang, Z. Liang, Y. Cao, Z. Han and X. Feng, *npj Flexible Electron.*, 2020, **4**, 2.
- 2 J. A. Rogers, T. Someya and Y. Huang, *Science*, 2010, **327**, 1603.
- 3 D. H. Kim, N. Lu, R. Ma, Y. S. Kim, R. H. Kim, S. Wang, J. Wu, S. M. Won, H. Tao, A. Islam, K. J. Yu, T. I. Kim, R. Chowdhury, M. Ying, L. Xu, M. Li, H. J. Chung, H. Keum, M. McCormick, P. Liu, Y. W. Zhang, F. G. Omenetto, Y. Huang, T. Coleman and J. A. Rogers, *Science*, 2011, **333**, 838.
- 4 M. Kaltenbrunner, T. Sekitani, J. Reeder, T. Yokota, K. Kuribara, T. Tokuhara, M. Drack, R. Schwodiauer, I. Graz, S. Bauer-Gogonea, S. Bauer and T. Someya, *Nature*, 2013, **499**, 458.
- 5 L. Shao, T. Lei, T. Huang, S. Li, T. Chu, M. Wong, R. Beausoleil, Z. Bao and K. Cheng, *IEEE Des. Test*, 2019, **36**, 6.
- 6 C. M. Boutry, L. Beker, Y. Kaizawa, C. Vassos, H. Tran, A. C. Hincley, R. Pfattner, S. Niu, J. Li, J. Claverie, Z. Wang, J. Chang, P. M. Fox and Z. Bao, *Nat. Biomed. Eng.*, 2019, **3**, 47.
- 7 K. Kwon, J. U. Kim, Y. J. Deng, S. R. Krishnan, J. Choi, H. Jang, K. H. Lee, C. J. Su, I. Yoo, Y. X. Wu, L. Lipschultz, J. H. Kim, T. S. Chung, D. R. Wu, Y. Park, T. I. Kim, R. Ghaffari, S. Lee, Y. G. Huang and J. A. Rogers, *Nat. Electron.*, 2021, **4**, 302.
- 8 K. S. Chun, Y. J. Kang, J. Y. Lee, M. Nguyen, B. Lee, R. Lee, H. H. Jo, E. Allen, H. Chen, J. Kim, L. Yu, X. Ni, K. Lee, H. Jeong, J. Lee, Y. Park, H. U. Chung, A. W. Li, P. A. Lio,

- A. F. Yang, A. B. Fishbein, A. S. Paller, J. A. Rogers and S. Xu, *Sci. Adv.*, 2021, 7, eabf9405.
- 9 L. Wang, K. Jiang and G. Shen, *Adv. Mater. Technol.*, 2021, 2100107.
- 10 S. Y. Chung, S. Kim, J.-H. Lee, K. Kim, S.-W. Kim, C.-Y. Kang, S.-J. Yoon and Y. S. Kim, *Adv. Mater.*, 2012, 24, 6022.
- 11 A. Wang, Z. Liu, M. Hu, C. Wang, X. Zhang, B. Shi, Y. Fan, Y. Cui, Z. Li and K. Ren, *Nano Energy*, 2018, 43, 63.
- 12 Y. Yang, W. Guo, K. C. Pradel, G. Zhu, Y. Zhou, Y. Zhang, Y. Hu, L. Lin and Z. L. Wang, *Nano Lett.*, 2012, 12, 2833.
- 13 K. Liu, T. Ding, J. Li, Q. Chen, G. Xue, P. Yang, M. Xu, Z. L. Wang and J. Zhou, *Adv. Energy Mater.*, 2018, 8, 1702481.
- 14 F.-R. Fan, Z.-Q. Tian and Z. L. Wang, *Nano Energy*, 2012, 1, 328.
- 15 W. T. Cao, H. Ouyang, W. Xin, S. Y. Chao, C. Ma, Z. Li, F. Chen and M. G. Ma, *Adv. Funct. Mater.*, 2020, 30, 2004181.
- 16 Y. Wang, Y. Yang and Z. L. Wang, *npj Flexible Electron.*, 2017, 1, 10.
- 17 Z. L. Wang, *Mater. Today*, 2017, 20, 74.
- 18 G. Zhu, Y. S. Zhou, P. Bai, X. S. Meng, Q. Jing, J. Chen and Z. L. Wang, *Adv. Mater.*, 2014, 26, 3788.
- 19 D. Choi, D. Yoo and D. S. Kim, *Adv. Mater.*, 2015, 27, 7484.
- 20 C. Dong, A. Leber, T. Das Gupta, R. Chandran, M. Volpi, Y. Qu, T. Nguyen-Dang, N. Bartolomei, W. Yan and F. Sorin, *Nat. Commun.*, 2020, 11, 3537.
- 21 M. Seol, S. Kim, Y. Cho, K.-E. Byun, H. Kim, J. Kim, S. K. Kim, S.-W. Kim, H.-J. Shin and S. Park, *Adv. Mater.*, 2018, 30, 1801210.
- 22 H. Zou, Y. Zhang, L. Guo, P. Wang, X. He, G. Dai, H. Zheng, C. Chen, A. C. Wang, C. Xu and Z. L. Wang, *Nat. Commun.*, 2019, 10, 1427.
- 23 H. Zou, L. Guo, H. Xue, Y. Zhang, X. Shen, X. Liu, P. Wang, X. He, G. Dai, P. Jiang, H. Zheng, B. Zhang, C. Xu and Z. L. Wang, *Nat. Commun.*, 2020, 11, 2093.
- 24 I. J. Chung, W. Kim, W. Jang, H.-W. Park, A. Sohn, K.-B. Chung, D.-W. Kim, D. Choi and Y. T. Park, *J. Mater. Chem. A*, 2018, 6, 3108.
- 25 S. S. K. Mallineni, H. Behlow, Y. Dong, S. Bhattacharya, A. M. Rao and R. Podila, *Nano Energy*, 2017, 35, 263.
- 26 X. Xia, J. Chen, G. Liu, M. S. Javed, X. Wang and C. Hu, *Carbon*, 2017, 111, 569.
- 27 H. S. Kim, D. Y. Kim, J. H. Kwak, J. H. Kim, M. Choi, D. H. Kim, D. W. Lee, D. S. Kong, J. Park, S. Jung, G.-H. Lee, M. Lee and J. H. Jung, *Nano Energy*, 2019, 56, 338.
- 28 H. Hwang, K. Y. Lee, D. Shin, J. Shin, S. Kim and W. Choi, *Appl. Surf. Sci.*, 2018, 442, 693.
- 29 I. Kim, H. Jeon, D. Kim, J. You and D. Kim, *Nano Energy*, 2018, 53, 975.
- 30 D. Kim, B. Pramanick, A. Salazar, I.-W. Tcho, M. J. Madou, E. S. Jung, Y.-K. Choi and H. Hwang, *Adv. Mater. Technol.*, 2016, 1, 1600160.
- 31 Y. J. Fan, X. S. Meng, H. Y. Li, S. Y. Kuang, L. Zhang, Y. Wu, Z. L. Wang and G. Zhu, *Adv. Mater.*, 2017, 29, 1603115.
- 32 J. Lin, Z. Peng, Y. Liu, F. Ruiz-Zepeda, R. Ye, E. L. G. Samuel, M. J. Yacaman, B. I. Yakobson and J. M. Tour, *Nat. Commun.*, 2014, 5, 5714.
- 33 R. Ye, D. K. James and J. M. Tour, *Adv. Mater.*, 2019, 31, 1803621.
- 34 L. Zhang, J. Tang, S. Liu, Q. Peng, R. Shi, B. N. Chandrashekar, Y. Li, X. Li, X. Li, B. Xu and C. Cheng, *Mater. Today Energy*, 2017, 5, 222.
- 35 S. A. Shankaregowda, R. F. S. M. Ahmed, C. B. Nanjegowda, J. Wang, S. Guan, M. Puttaswamy, A. Amini, Y. Zhang, D. Kong, K. Sannathammegowda, F. Wang and C. Cheng, *Nano Energy*, 2019, 66, 104141.
- 36 S. Mao, G. Lu and J. Chen, *Nanoscale*, 2015, 7, 6924.
- 37 B. Luo and L. Zhi, *Energy Environ. Sci.*, 2015, 8, 456.
- 38 R. Ye, Z. Peng, T. Wang, Y. Xu, J. Zhang, Y. Li, L. G. Nilewski, J. Lin and J. M. Tour, *ACS Nano*, 2015, 9, 9244.
- 39 G. Cai, Z. Yu, R. Ren and D. Tang, *ACS Sens.*, 2018, 3, 632.
- 40 M. Dosi, I. Lau, Y. Zhuang, D. S. A. Simakov, M. W. Fowler and M. A. Pope, *ACS Appl. Mater. Interfaces*, 2019, 11, 6166.
- 41 M. G. Stanford, J. T. Li, Y. Chyan, Z. Wang, W. Wang and J. M. Tour, *ACS Nano*, 2019, 13, 7166.
- 42 C. Jiang, X. Li, Y. Yao, L. Lan, Y. Shao, F. Zhao, Y. Ying and J. Ping, *Nano Energy*, 2019, 66, 104121.
- 43 P. Zhao, G. Bhattacharya, S. J. Fishlock, J. G. M. Guy, A. Kumar, C. Tsonos, Z. Yu, S. Raj, J. A. McLaughlin, J. Luo and N. Soin, *Nano Energy*, 2020, 75, 104958.